THERMOCOUPLE THERMAL INERTIA DURING REFUELING OF HYDROGEN TANKS: CFD VALIDATION

Ren V.[1], Lodier G.[1], Ammouri F.[1]
[1] Air Liquide, Innovation Campus Paris, 1 chemin de la Porte des Loges, Les-Loges-en-Josas, 78350, France, vincent.ren@airliquide.com

ABSTRACT

Fueling and defueling of hydrogen composite tanks is an important issue for the safe handling of hydrogen. To prevent temperature rise during refuelling (maximum allowed T=+85°C), the rate of fueling must be carefully controlled. Using Computational Fluid Dynamics (CFD), we simulate the temperature and velocity distribution inside the tank during these processes, including cases where thermal stratification occurs. Simulations of two tank configurations with tilted injectors are presented, along with experimental data validation. A model is proposed to account for the thermal inertia of the thermocouples, making it possible to compare more reliably CFD results with experimental measurements.

1.0 INTRODUCTION

Gaseous hydrogen has the potential to enter the transportation sector by offering a clean and efficient alternative to conventional fossil fuels. However, the successful deployment of hydrogen fuel cell vehicles requires a safe and reliable refueling protocol. The SAE J 2601 is one standard for safe heavy duty vehicles fueling protocols.

For instance, a key objective for composite tanks is to control the rate of fueling to avoid overheating, with a limit temperature of 85°C in the liner. Above this temperature, the liner lifetime could be drastically reduced. 0D and 1D models have been developed to this purpose [1]–[6]. However, in some refueling conditions, temperature stratification can be observed and the temperature can locally exceed 85°C [7]. To understand and eventually to avoid the onset of such non-homogeneities, 3D CFD (Computational Fluid Dynamics) simulations are required to simulate the flow behavior inside the tank. Among all parameters, the configuration of the injector plays a major role in the resulting flow patterns inside the tank, as it determines the velocity and the direction of the injection jet. CFD studies have been performed both on tanks with straight injector [8]–[15] and tilted injectors [16]–[19].

The validation of the simulations is often based on experimental data obtained with a thermocouple tree immersed in the gas. However, due to its thermal inertia, the thermocouples measure a time-filtered value of the gas temperature leading to a delay and a damping of the high frequencies of the time-fluctuations of the temperature. In this work, a model is proposed to correct the CFD simulations by applying a physics-based transformation of the local temperature time evolution. The CFD results including this correction are presented for two refueling cases and compared to experimental measurements issued from the PRHYDE project [20].

The first case includes an injector tilted upwards and a detailed CFD study has been done to reproduce at best the experimental data in [19]. This work focuses only on the impact of the thermocouple delay correction in this case.

In the second case, an injector tilted upwards and sidewise is considered. The same simulation and correction methodology is applied as for the first case and the results are compared with the experimental data. In addition, specific attention is paid to the analysis of the temperature evolution in the vicinity of the on tank valve (OTV). This measurement is key as it is used to monitor the conditions of the refueling protocol. Consequently, it should be representative of the averaged gas temperature.

2.0 DESCRIPTION OF THE PROBLEM

Two refuelling cases with two different tanks and fueling conditions are studied in this work. In the following, they will be referred as “case 1” and “case 2”.

2.1 Tank geometries

The tank used are Hexagon tanks respectively of 165L and 240L for case 1 and 2. Both are type IV tanks, meaning that they are made of a liner in plastic and a wrapping in composite. The 3D geometry and the different materials are described Fig. 1. It can be noticed that the Hexagon 165L tank used for case 1 has a much greater L/D aspect ratio than the Hexagon 240L tank used for case 2, namely 8.2 vs 3.7.

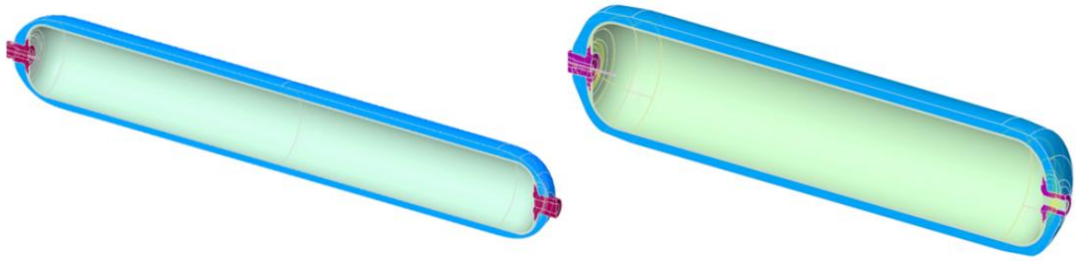

Figure 1. 3D view of half of the tanks: Hexagon 165L (left) and Hexagon 240L (right). The colors correspond to different materials: liner in light blue, composite wrapping in blue, inboss and endboss in purple.

Another difference between both tanks is their injector geometry. In both cases, the tip of the injector is tilted upward to avoid the onset of vertical temperature stratification. However, in case 2, the injector is also tilted sidewise, see Fig. 2.

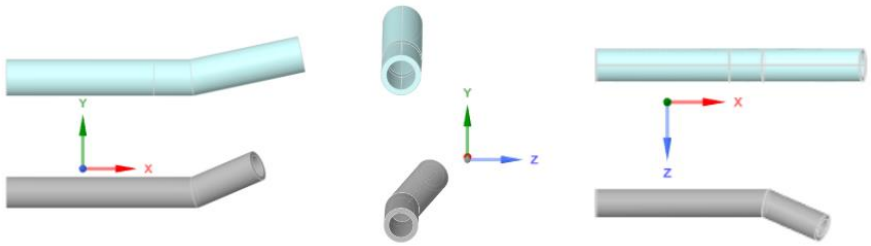

Figure 2. Different views of the injectors in case 1 (cyan) and case 2 (gray). From left to right: side, back and top

2.2 Test conditions

Several experimental tests with varying refueling conditions have been performed on both tanks [20]. Due to the high computational cost of a CFD simulation, only 2 cases have been selected for validation. The test corresponding to case 1 has been selected for CFD study due to the high thermal stratification, in order to assess the capability of CFD to capture this thermal regime. Among all the tests performed on the second tank, the test corresponding to case 2 has been selected because high amplitude temperature oscillations (around 10°C) were observed around the OTV (see Fig. 3). These unstable measurements can be an issue for refueling monitoring purposes. One of the objectives for the CFD modelling is to eventually reproduce and understands these oscillations.

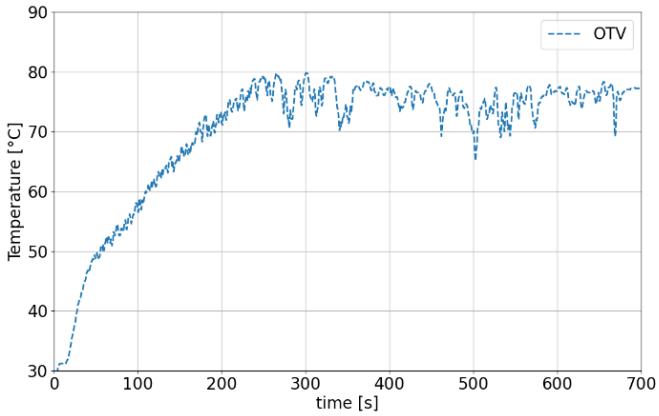

Figure 3. Time evolution of the OTV temperature measurement for case 2.

The refueling conditions for each test are given in Table 1 and the time evolution of the inlet boundary conditions are provided in Fig.4 for case 1 and Fig. 5 for case 2. The tank inlet temperature is calculated from a temperature measurement 2m upstream the tank, taking into account the heat losses and the inertia of the pipes. The mass flow rate is deduced from the pressure profiles. The oscillations for case 3 could come from leak tests done during the experiment. For both cases, the hydrogen is precooled to limit the maximum gas temperature in the tank.

Table 1. Tests conditions for case 1 and case 2.

Case	Initial pressure [bar]	Ambient temperature [°C]	Precooling temperature [°C]	Pressure profile [MPa/min]	Final pressure [bar]	Final temperature [°C]	Fueling time [s]	Volume of the tank [L]
1	20	50	-40	8	700	75	600	165
2	20	30	-30	20	700	75	700	240

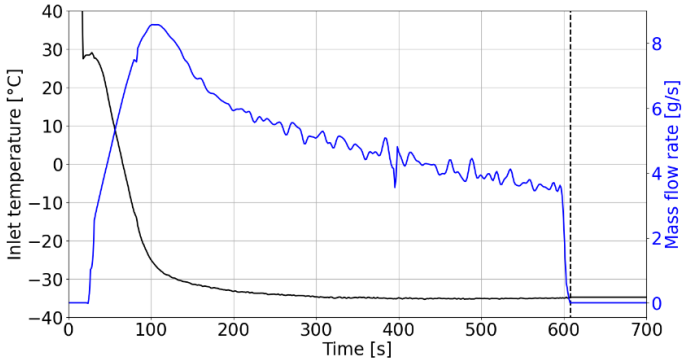

Figure 4. Time evolution of the inlet temperature (black) and mass flow rate (blue) for case 1.

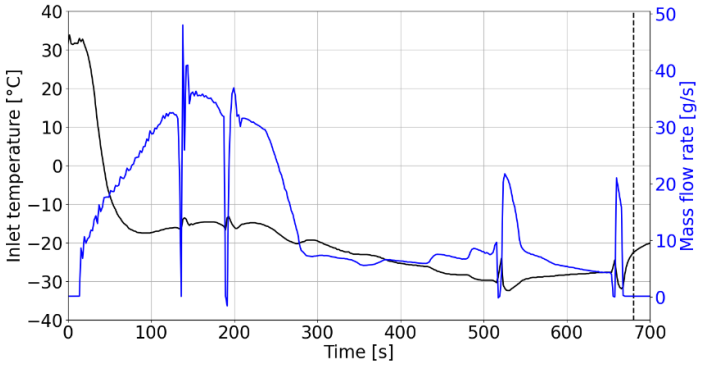

Figure 5. Time evolution of the inlet temperature (black) and mass flow rate (blue) for case 2.

2.3 Temperature measurements

In both experimental tests, the tanks were equipped with a thermocouple tree with 16 thermocouples inside the tank. They are of type T with a tip of 1mm diameter. The locations and the tag of these probes are shown Fig. 6.

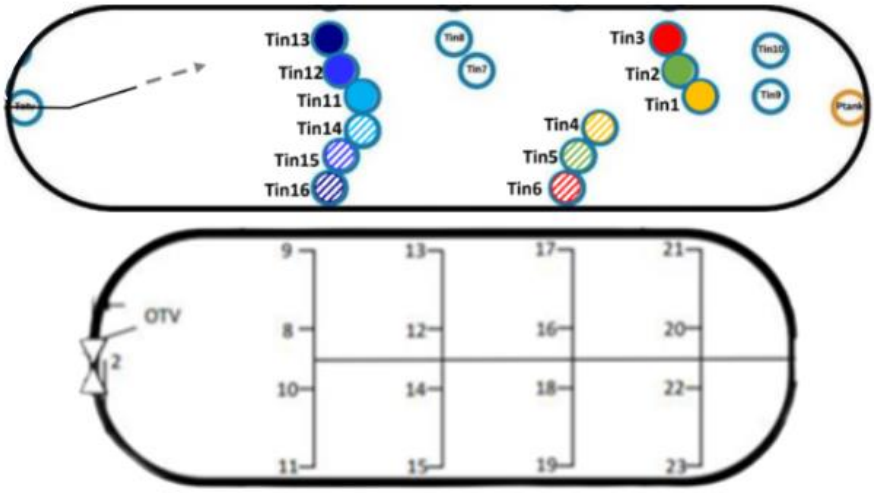

Figure 6. Location of the various thermocouples equipping the tanks for case 1 (top) and case 2 (bottom)

Fig. 7 shows the time-evolution of the experimental measurements for both case 1 and case 2. A large horizontal thermal stratification can be observed in case 1 (around 25°C at 100s) with temperatures exceeding 85°C for some thermocouples in the back of the tank, see T1, T2, T3 and T9, T10, while the thermocouples in the front are cold, see T11, 12, 13. For case 2, a horizontal thermal stratification is also observed but with a much smaller amplitude (around 10°C).

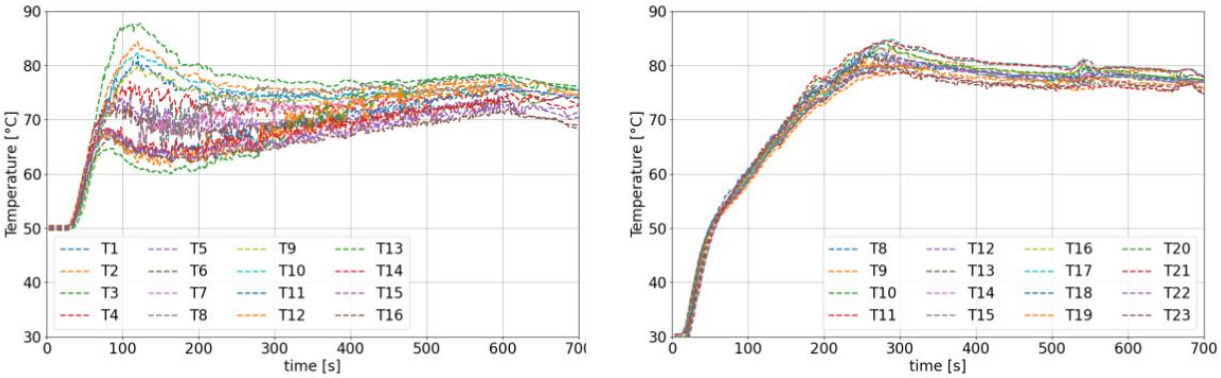

Figure 7. Time evolution of the temperature measured by the thermocouples. Left: case 1. Right: case 2. Refer to Fig. 6 for the thermocouple tags correspondence.

3.0 METHODOLOGY

3.1 Numerical modelling

The simulated domain consists in the hydrogen tank and the fluid domain inside. For case 1, only half of the tank is considered, making use of the vertical symmetry plan. The whole tank volume has to be considered for case 2 because of the sidewise tiling of the injector. The calculations were done with ANSYS Fluent v19R2.

The methodology used for the mesh is similar for both cases. The mesh is mainly hexahedral with refinements inside and outside of the injector and in the boundary layers of the inner wall of the tank. Indeed, accurate description of the jet dynamics is key to predicting stratification. It impacts the momentum and energy exchange with the surrounding gas and at the wall impingement. To give a quantitative an idea of the mesh, the injector pipe contains 5 cells along its diameter, the maximum y+ in the boundary layer of the inner tank wall is 10 and the total number of cells is around 800,000 for both cases. Fig. 8 shows a snapshot of the mesh for each case.

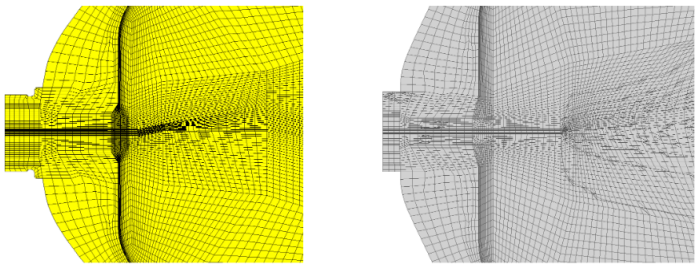

Figure 8. View of the mesh on a vertical slice near the injector. Left: case 1. Right case 2.

In the fluid domain, Unsteady Reynolds-averaged Navier-Stokes (U-RANS) equations are solved with the Reynolds Stress Model (RSM) turbulence model with standard wall functions. This model has shown good performances on these tilted injector configurations with an impinging jet [19]. In each solid domain, the unsteady energy equation is solved to include the heat conduction contribution.

The inlet temperature and mass flow rate shown in Fig. 4 and Fig. 5 are used as unsteady boundary conditions for the fluid domain. Convective and radiative boundary conditions is imposed to model the heat transfer between the external walls and the environment. The convective heat transfer coefficient is extracted from a preliminary 0D/1D simulation with SOFIL.

The REFPROP database from the National Institute of Standards and Technology (NIST) is used for the hydrogen equation of state. The solid properties are taken from [4], based on experimental measurements.

3.2 Thermocouples measurements delay

A thermocouple is constituted of two different wires electrically insulated along of its length. These two wires are welded at the thermocouple extremity where the temperature is measured. In general, the thermocouple is sheathed on all of its length to protect the welding and the two wires from direct contact with the gas and from potential mechanical or chemical degradation. The thermocouple sheath is often made from stainless steel and is electrically insulated of the welding and the two wires.

By principle, the thermocouple measurement gives the temperature of the welding point. However, the thermocouple is generally used to measure the fluid temperature around its extremity. Consequently, our need is to estimate the difference between the thermocouple measurement and the fluid temperature around especially in unsteady state case, a typical situation during a tank filling and emptying.

To carry out this estimation, an energy balance equation is applied on the thermocouple extremity.

$$m_t \, Cp_t \frac{dT_t(t)}{dt} = \; k_t(t) \; S_t \; \Big(T_g(t) - T_t(t)\Big), \tag{1}$$

where m_t, Cp_t, T_t, k_t, and S_t are respectively the thermocouple properties for mass, specific heat capacity, temperature, convective heat transfer coefficient around the thermocouple and external surface and T_g is the gas temperature around the thermocouple and t the time.

We can introduce the convection characteristic time around the thermocouple $\tau_{cv}(t)$ which is time dependent due to the heat transfer coefficient dependence on time.

$$\tau_{cv}(t) = \frac{m_t\, Cp_t}{k_t(t)\, S_t} = \frac{\rho_t\, V_t\, Cp_t}{k_t(t)\, S_t} \approx \frac{\rho_t\ d_t\, Cp_t}{4\, k_t(t)}, \tag{2}$$

where d_t is a characteristic length for the isothermal part. In this work, d_t = 7 mm is the thickness of the thermocouple tree (see Fig. 9). To calculate $k_t(t)$, we will use the Nusselt number Nu_{d_t} correlation based on thermocouple diameter for external forced convection around a cylinder submitted to gas crossflow [21] that can be expressed in the form:

$$Nu_{d_t} = 0.3 + \frac{0.62\ Re_{d_t}^{1/2} Pr^{1/3}}{\left[1+\left(\frac{0.4}{Pr}\right)^{2/3}\right]^{1/4}} \left[1 + \left(\frac{Re_{d_t}}{282000}\right)^{5/8}\right]^{4/5}, \tag{3}$$

The last equation is valid for the entire range of Reynolds number $Re_{d_t} = \frac{\rho_g v_g d_t}{\mu_g}$ (based on thermocouple diameter and the gas local velocity v_g across the thermocouple) and for Prandtl number Pr higher or equal to 0.2 which is the case for almost all gases and especially for hydrogen gas. ρ_g and μ_g are respectively the gas density and dynamic viscosity at the film temperature (average between gas and wall temperature) around the thermocouple. All other gas thermo-physical properties in the last equation are calculated using the film temperature around the thermocouple. Then we can deduce the convection heat transfer coefficient using the definition of the Nusselt number.

$$k_t = \frac{Nu_{d_t}\, \lambda_g}{d_t}, \tag{4}$$

where λ_g is the thermal conductivity of the gas at film temperature around the thermocouple.

Using equations (1) and (3), one can write:

$$\frac{dT_t(t)}{dt} = \frac{T_g(t) - T_t(t)}{\tau_{cv}(t)}, \tag{5}$$

with the initial conditions $T_t(0) = T_g(0) =$ Initial temperature of the tank, which is often equal to ambient temperature and $k_t(0)$ is low as the Nusselt number is very low (0.3) since the gas initial velocity inside the tank is zero everywhere.

As a results, from the gas local temperature calculated using CFD, one can deduce the thermocouple temperature in function of time using equation (5) using the calculated gas local velocity. The more the gas velocity is locally high, the more the convection transfer coefficient around the thermocouple is high and the more the convection time characteristic is low. Then the more the thermocouple will follow rapidly the gas temperature variations.

Figure 9. Side view of the thermocouple tree used in case 1.

For future experiments, it could be interesting to calibrate the thermocouples under different temperature and velocity conditions.

4.0 RESULTS AND DISCUSSIONS

4.1 Case 1: horizontal filling with an injector tilted upwards

The simulation results have already been discussed in [19] and fairly good temperature predictions results have been observed. The objective here is to apply the previously described transformation on the simulation results and evaluate the improvement of the results accuracy with respect to the measurements.

Fig. 10 shows the temperature and velocity contours at a time when high horizontal temperature stratification occurs. The cold jet impinges the top wall and falls down at half the tank, because the buoyancy forces generated by the density gradient dominate over its inertia. Two different flow regimes are then observed in each zone of the tank. In the front, the cold gas recirculates with high velocities while a hot zone with very low velocity is created in the back of the tank.

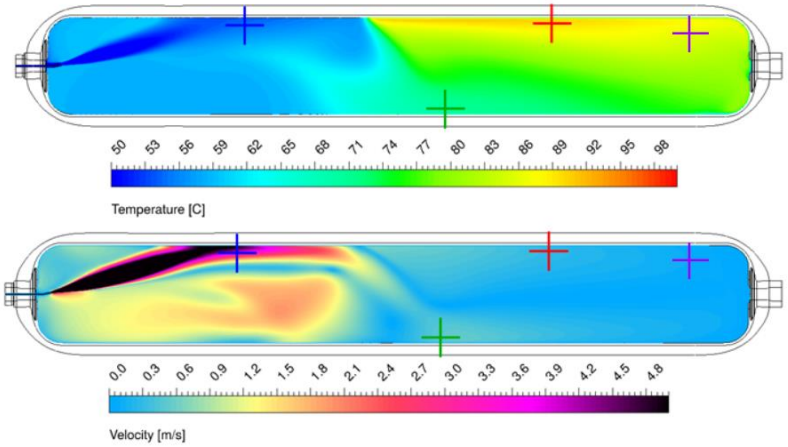

Figure 10. Gas temperature (top) and velocity magnitude (bottom) contours at t=100s. The blue, red, green and violet crosses correspond respectively to the thermocouple 13, 3, 6 and 10.

Thermocouples 3 and 10 that are located in the top back of the tank are immersed in a low velocity region of the tank, namely approximately 0.2 m/s for T3 and 0.05 m/s for T10, see Fig. 11. As a result, the correction is applied with a long delay and the difference with the raw simulation results is large. The characteristic time scale of the delay is of the order of several tens of seconds. The corrected CFD results are in better agreement with the experiment. On the other hand, thermocouple 13 is located in the jet trajectory, in an area with high velocities. Under these conditions, the correction has almost no impact on the results. The numerically predicted temperature remains colder than the experimentally measured one.

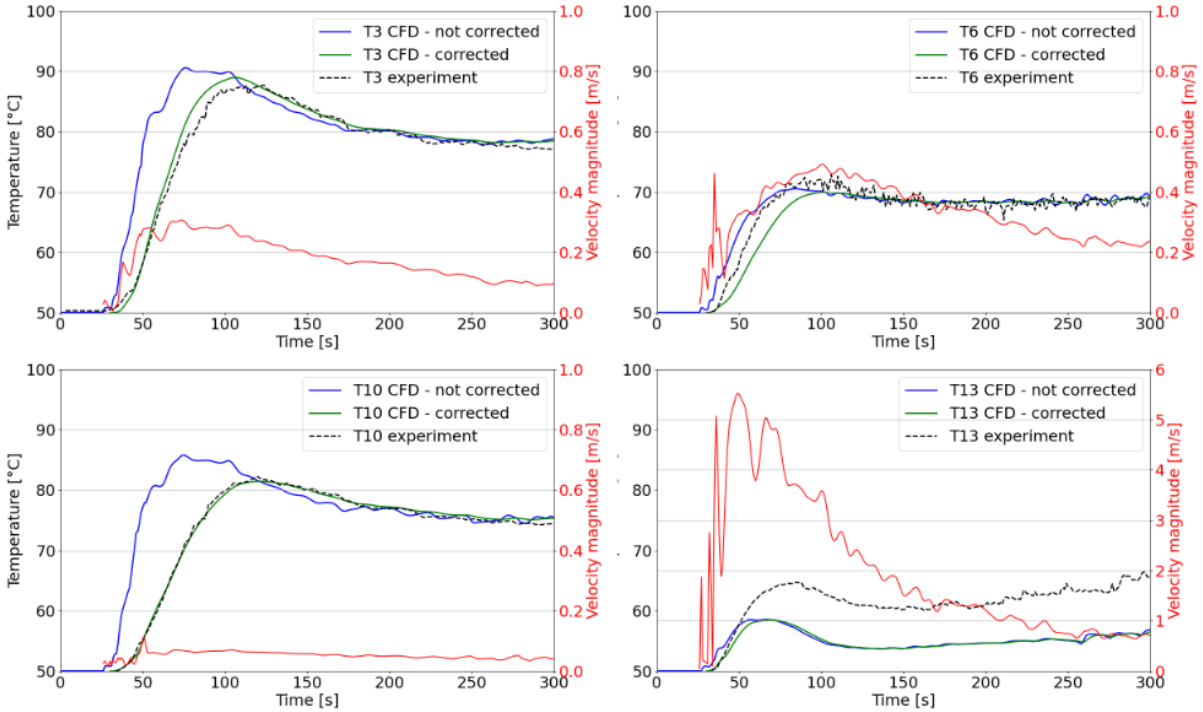

Figure 11. Comparison between experimentally measured temperature (dashed black line), raw simulation results (blue) and simulation results corrected with a delay based on the simulated local velocity (green). Refer to Fig. 6 for the location of the thermocouples.

4.2 Case 2: horizontal filling with an injector tilted upwards and sidewise

The same methodology has been applied to case 2. The temperature levels measured by the third row of thermocouples are presented in Fig. 13. As for case 1, the velocity magnitude is lower in the back of the tank than in its front part, see Fig. 12. Consequently, the correction has a low effect on T10 and T14 while delays up to 30s can be observed on T18 and T22. These corrections are coherent when comparing with the experimental data in the first 300 seconds, see Fig. 13. For T10 and T14, the numerical results are not significantly impacted but the delaying effect of the temperature correction makes it possible to obtain better agreement with the experimental measurements. It also damps the higher frequency fluctuation in accordance with experimental observations. After 300s, the simulation overestimates the temperature levels by approximately 5°C for all the thermocouples. This overall error may be related to an underestimation of the heat transfer coefficient between the walls and the exterior, or the walls and the fluid. Only the first 400s are shown in the plots to better visualize the thermocouple delay. After 400s, the temperatures and the stratification are steady, in agreement with the experiment.

The onset of a horizontal temperature stratification can be observed at 100s on Fig. 12, similarly to case 1. Fig. 13 provides a more quantitative idea of this stratification. It shows the temperature difference between thermocouples T9 and T23, located at two opposite axial positions. Two phases can thus be identified, with a transition at around 280s. In a first phase, a horizontal temperature stratification is observed with an amplitude of around 5°C. In a second phase, this stratification regime disappears. The qualitative change is well captured by the CFD.

Fig. 15 shows streamlines colored by the x-component of the velocity at a time step in the first phase (t=200s). A flow pattern similar to case 1 is observed. The cold jet hits the top of the tank and falls because of buoyancy forces, leading to the appearance of a recirculation zone in the front of the tank. The viscous shearing induced by this first recirculation zone is at the origin of a second one in the back of the tank. As a results, the two zones exchanges littles gas with each other, preventing the back area of the tank to be cooled down by the injected cold hydrogen.

After 280s, the inlet velocity is much lower, see Fig. 14. A new flow topology is observed, see Fig. 16. The lower jet velocity levels lead to weakened recirculation zones, both in the front and back areas of the tank. A greater part of the injected cold gas is thus transported to the back and mixes with the hot gas parcels, resulting in a homogeneous thermal regime.

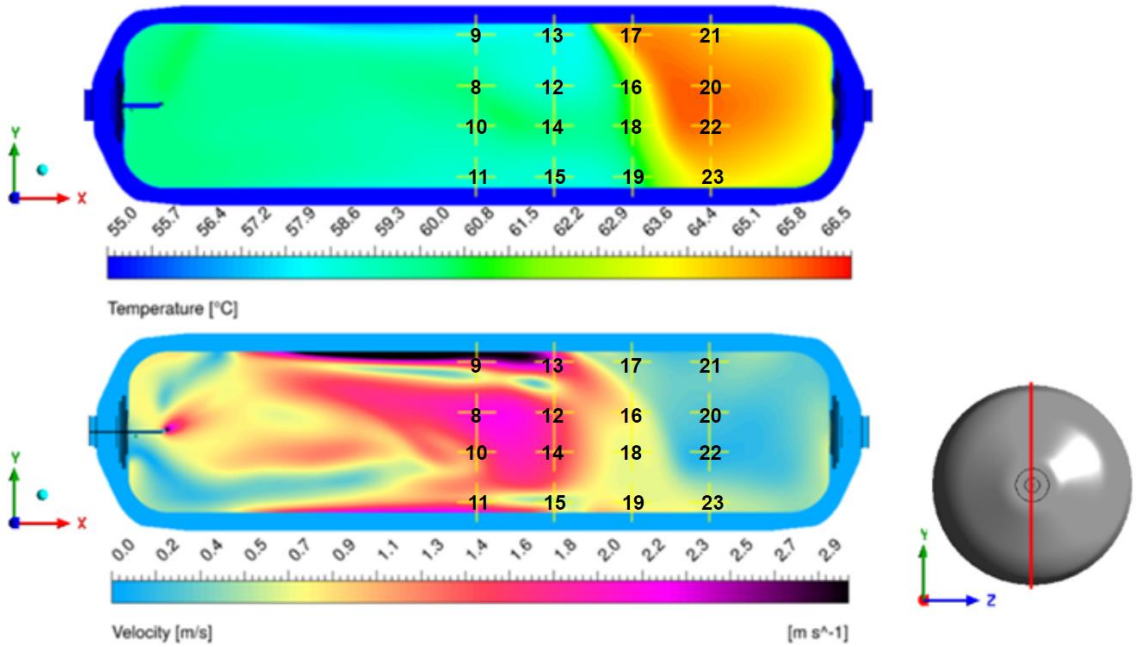

Figure 12. Gas temperature and velocity magnitude contours at 100s. The yellow crosses corresponds to the thermocouple positions.

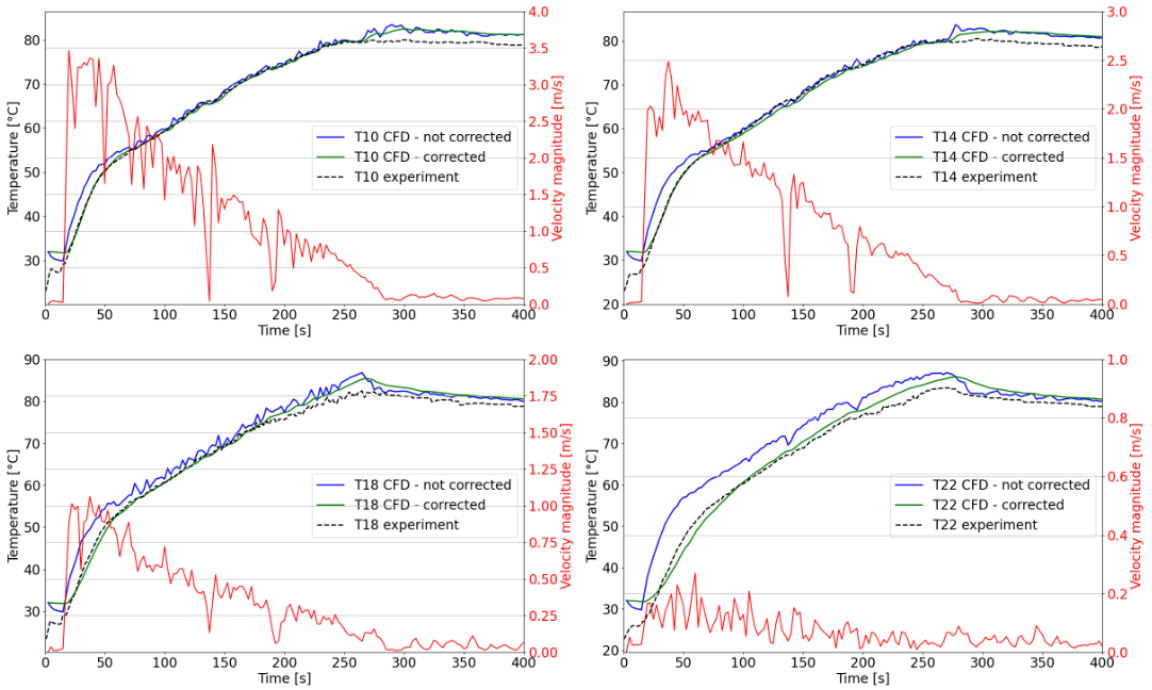

Figure 13. Comparison between experimentally measured temperature (dashed black line), raw simulation results (blue) and simulation results corrected with a delay based on the simulated local velocity (green). Refer to Fig. 6 for the location of the thermocouples.

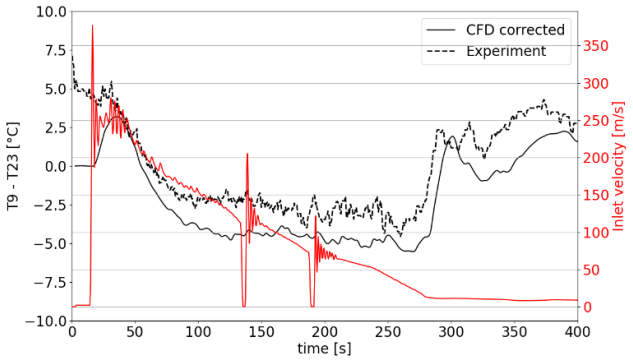

Figure 14. Comparison of the temperature stratification between CFD (corrected) and experiment.

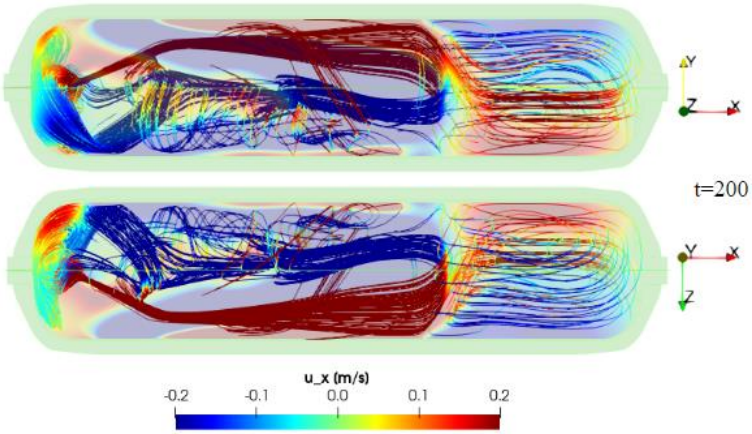

Figure 15. Horizontal velocity field and streamlines at 200s. Top: side view, bottom: top view.

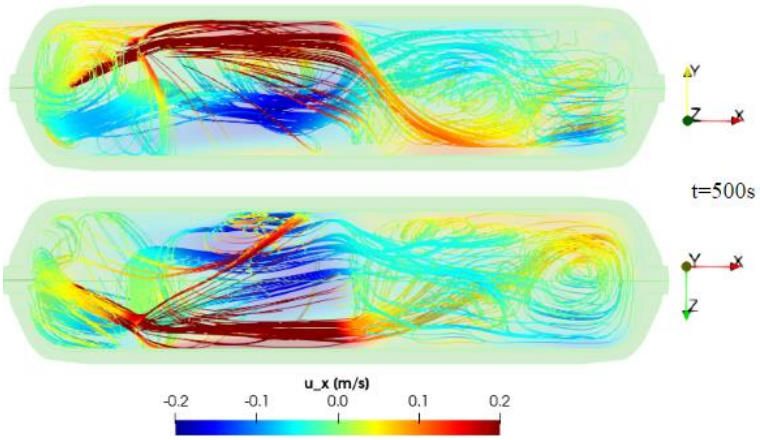

Figure 16. Horizontal field and streamlines at 500s. Top: side view, bottom: top view.

The OTV measurement is a key indicator to monitor the conditions of the refueling protocol. As such, it should be representative of the average gas temperature. Another objective of the present CFD study is to understand the measured time-fluctuations in temperature levels at the OTV in case 2. The right picture in Fig. 17 shows the corresponding measured and computed temperatures. The amplitude and the frequency of the measured temperature after 280s are fairly well captured by the simulation. The figure on the left displays streamlines colored by the temperature in the vicinity of OTV. At this location, a shear layer between a downward cold stream and an upward hot recirculating stream can be observed. This results in a hydrodynamic instability leading to the observed temperature fluctuations, thus

suggesting that the chosen location is not adapted to capture the average temperature. A frequency analysis could be interesting, keeping in mind that the high frequency fluctuations are filtered by the thermocouples.

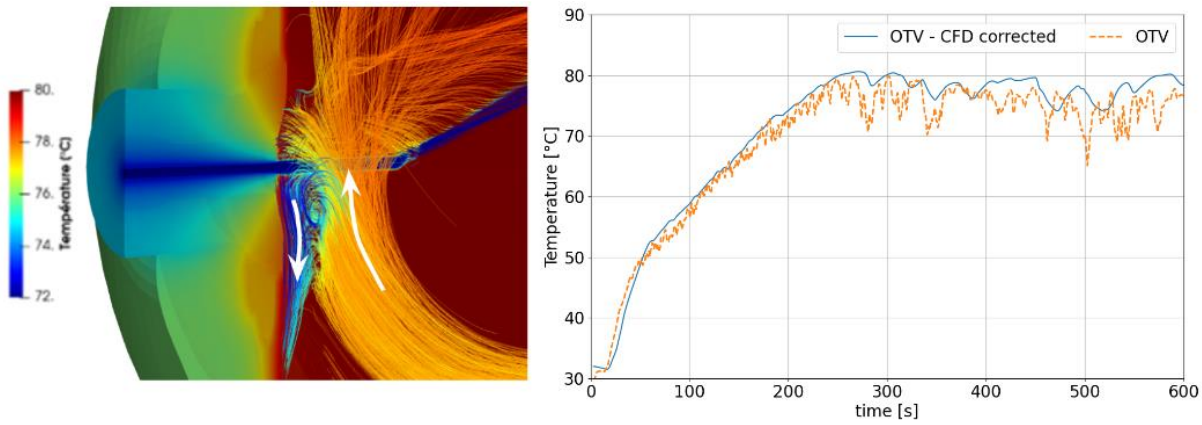

Figure 17. Left: Streamlines colored by temperature near the injector. The arrows indicate the direction of the flow. Right: temperature just underneath the injector pipe.

5.0 CONCLUSION

Two CFD studies have been conducted on horizontal tank refueling with tilted injectors. In both cases, a hot dead zone (i.e. a zone with low turbulent activity) is created in the back of the tank and horizontal stratification is observed. The stratification disappears at the end of the filling when the injection velocities decreases, but for different reasons. In the first case, the injector is tilted upwards and the stratification disappears as the jet impingement with the top of the tank ends. In the second case, the injector is tilted upwards and sidewise and the stratification disappears when the two counter-rotating recirculation zones weaken because of lower jet injection velocity levels. This complex phenomenology show that the commonly used 5 m/s criteria to determine temperature stratification [2] does not easily apply to tilted injectors. Also, further work could be done to determine a better location for the OTV for these configurations.

For both cases, in the dead zone, the thermocouples measure temperatures with a higher delay due to their thermal inertia. A methodology has been proposed to take into account this effect when comparing simulated gas temperatures and experimental measurements. For the two cases under interest in this work, delays up to 30 seconds have been estimated. Part of the departure between the numerical and the experimental results has been recovered thank to this correction.

As perspectives, similar tests and simulations could be done for fast defueling cases, where temperature below -40°C should be avoided in the tank walls.

ACKNOLEDGEMENTS

This work has been achieved in the framework of a project which has received funding from the Fuel Cells and Hydrogen 2 Joint Undertaking (now Clean Hydrogen Partnership) under Grant Agreement No 874997. This Joint Undertaking receives support from the European Union's Horizon 2020 Research and Innovation program, Hydrogen Europe and Hydrogen Europe Research. We thank all partners of the PRHYDE project for their contribution to this work, namely: Air Liquide, CEA, ENGIE, ITM, NEL, Nikola, Toyota Europe and Toyota North America, Shell, ZBT, and LBST. The work was also co-funded by Air Liquide itself.

REFERENCES

1. J. C. Yang, A thermodynamic analysis of refueling of a hydrogen tank, *Int. J. Hydrog. Energy*, **34**, No. 16, 2009, pp. 6712–6721
2. T. Bourgeois, F. Ammouri, M. Weber, and C. Knapik, Evaluating the temperature inside a tank during a filling with highly-pressurized gas, *Int. J. Hydrog. Energy*, **40**, No. 35, 2015, pp. 11748–11755
3. F. Olmos and V. I. Manousiouthakis, Hydrogen car fill-up process modeling and simulation, *Int. J. Hydrog. Energy*, **38**, No. 8, 2013, pp. 3401–3418
4. T. Bourgeois *et al.*, Optimization of hydrogen vehicle refuelling requirements, *Int. J. Hydrog. Energy*, **42**, No. 19, 2017, pp. 13789–13809
5. T. Bourgeois, F. Ammouri, D. Baraldi, and P. Moretto, The temperature evolution in compressed gas filling processes: A review, *Int. J. Hydrog. Energy*, **43**, 2018
6. E. Ruffio, D. Saury, and D. Petit, Thermodynamic analysis of hydrogen tank filling. Effects of heat losses and filling rate optimization, *Int. J. Hydrog. Energy*, **39**, No. 24, 2014, pp. 12701–12714
7. T. Terada, H. Yoshimura, Y. Tamura, H. Mitsuishi, and S. Watanabe, Thermal Behavior in Hydrogen Storage Tank for FCV on Fast Filling (2nd Report), SAE International, Warrendale, PA, SAE Technical Paper 2008-01–0463, 2008.
8. P. Carrere, G. Lodier, E. Vyazmina, F. Ammouri, A. Charolais, and R. Gonin, CFD Simulations of the Refueling of Long Horizontal H2 Tanks, 2021
9. R. Gonin *et al.*, A computational fluid dynamic study of the filling of a gaseous hydrogen tank under two contrasted scenarios, *Int. J. Hydrog. Energy*, **47**, No. 55, 2022, pp. 23278–23292
10. J.-Q. Li, J.-C. Li, J.-T. Kwon, and C. Shang, The effect of internal pressure change on the temperature rise and the amount of filling hydrogen of high pressure storage tank, *Adv. Mech. Eng.*, **14**, No. 8, 2022
11. S. Sapre, M. Vyas, and K. Pareek, Impact of refueling parameters on storage density of compressed hydrogen storage Tank, *Int. J. Hydrog. Energy*, **46**, No. 31, 2021, pp. 16685–16692
12. J. Zheng *et al.*, Experimental and numerical study on temperature rise within a 70 MPa type III cylinder during fast refueling, *Int. J. Hydrog. Energy*, **38**, 2013, pp. 10956–10962
13. A. Suryan, H. D. Kim, and T. Setoguchi, Comparative study of turbulence models performance for refueling of compressed hydrogen tanks, *Int. J. Hydrog. Energy*, **38**, No. 22, 2013, pp. 9562–9569
14. V. Ramasamy and E. S. Richardson, Thermal response of high-aspect-ratio hydrogen cylinders undergoing fast-filling, *Int. J. Heat Mass Transf.*, **160**, 2020, p. 120179
15. N. de Miguel, B. Acosta, D. Baraldi, R. Melideo, R. Ortiz Cebolla, and P. Moretto, The role of initial tank temperature on refuelling of on-board hydrogen tanks, *Int. J. Hydrog. Energy*, **41**, No. 20, 2016, pp. 8606–8615
16. D. Melideo, D. Baraldi, N. De Miguel Echevarria, and B. Acosta Iborra, Effects of some key-parameters on the thermal stratification in hydrogen tanks during the filling process, *Int. J. Hydrog. Energy*, **44**, No. 26, 2019, pp. 13569–13582
17. D. Melideo, D. Baraldi, M. E. N. De, and I. B. Acosta, Effects of the injector direction on the temperature distribution during filling of hydrogen tanks, *JRC Publications Repository*, Nov. 16, 2017. https://publications.jrc.ec.europa.eu/repository/handle/JRC105387
18. X. Wu, J. Liu, J. Shao, and G. Deng, Fast filling strategy of type III on-board hydrogen tank based on time-delayed method, *Int. J. Hydrog. Energy*, **46**, No. 57, 2021, pp. 29288–29296
19. J. Martin *et al.*, Influence of the turbulence model in the CFD simulation of hydrogen tank Filling by an impinging oblique jet [Manuscript submitted for publication]
20. Protocol for heavy duty hydrogen refuelling | PRHYDE Project | Fact Sheet | H2020 | CORDIS | European Commission. https://cordis.europa.eu/project/id/874997
21. S. W. Churchill and M. Bernstein, A Correlating Equation for Forced Convection From Gases and Liquids to a Circular Cylinder in Crossflow, *J. Heat Transf.*, **99**, No. 2, 1977, pp. 300–306